Orienting rigid and flexible biological assemblies in ferrofluids for small-angle neutron scattering studies

T. Sosnick,* S. Charles,‡ G. Stubbs,§ P. Yau,‖ E. M. Bradbury,*‖ P. Timmins,¶ and J. Trewhella*

*Life Sciences Division, Los Alamos National Laboratory, Los Alamos, New Mexico 87545; ‡Department of Chemistry, University College of North Wales, Bangor Gwynedd, Wales; §Department of Molecular Biology, Vanderbilt University, Nashville, Tennessee; ‖Department of Biological Chemistry, University of California at Davis, California USA; and ¶Institut Laue-Langevin, Grenoble Cedex, France

ABSTRACT Small-angle scattering from macromolecules in solution is widely used to study their structures, but the information content is limited because the molecules are generally randomly oriented and hence the data are spherically averaged. The use of oriented rodlike structures for scattering, as in fiber diffraction, greatly increases the amount of structural detail that can be obtained. A new technique using a ferromagnetic fluid has been developed to align elongated structures independent of their intrinsic magnetic properties. This technique is ideal for small-angle neutron scattering because the scattering from the ferrofluid particles can be reduced significantly by matching the neutron scattering length density of the particles to a D_2O solvent ("contrast matching"). The net result is scattering primarily from the ordered biological assembly in a solution environment that can be adjusted to physiological pH and ionic strength. Scattering results from ordered tobacco mosaic virus, tobacco rattle virus, and chromatin fibers are presented.

INTRODUCTION

The amount of structural information that can be derived from scattering studies on biological assemblies depends greatly upon the degree of order in the sample. The highest resolution information is obtained when the scattering is from a molecule, or molecular assembly, in a three-dimensional crystal. The resulting diffraction pattern can reveal the precise locations of individual chemical groups, or sometimes atoms, in the structure. At the other extreme, scattering from randomly oriented molecules in solution gives information about their overall shapes and interactions. In between these two extremes lie scattering studies from partially ordered systems. For example, certain rodlike biological assemblies will form fibers in which their long axes are oriented in one dimension. These types of structures generally will not crystallize in three dimensions for high resolution structural analysis, but scattering from the oriented fibers can give rise to diffraction peaks that can be assigned to structural repeats in particular directions. In special cases, for example when the biological assembly has an intrinsic symmetry such as in a helical structure, this one-dimensional ordering has resulted in the elucidation of three-dimensional structural details at the level of individual chemical groups. A historic example is the structure of the DNA double helix which was solved using a combination of model building and medium resolution x-ray diffraction data on drawn DNA fibers.

A more recent example of the use of fiber diffraction is the structure of the rodlike helical virus assembly, Tobacco Mosaic Virus (TMV). A complete three-dimensional structure of TMV at 2.9 Å resolution has been obtained using x-ray diffraction data from liquid crystal gels aligned by shearing forces (1, 2). TMV also possesses a sufficiently large intrinsic diamagnetic moment that the liquid crystal domains align in magnetic fields of about 20–30 kG (3, 4). Other biological assemblies such as purple membranes, whole retinal rods, nucleic acids, sickle cell hemoglobin fibers, and filamentous bacteriophages have also been oriented in large, 10–20 kG, magnetic fields for structural studies (reviewed in reference 5). However, most biological structures have neither sufficient diamagnetic anisotropy to result in orientation in readily obtainable magnetic fields, nor the appropriate morphological and electrostatic characteristics to align as a result of hydrodynamic shearing forces.

We have been developing a new technique for aligning rodlike biological assemblies independent of their intrinsic magnetic properties. This technique uses a ferromagnetic fluid (or ferrofluid) and modest, <5 kG, magnetic fields (6). The ferrofluid is composed of

Address correspondence to Dr. Trewhella.

Abbreviations used in this paper: DoF, degrees of freedom; HOS, higher order structure; D, sample to detector distance; DFF, deuterated ferrofluid; EDTA, Ethylenediaminetetraacetic acid; H, Magnetic field; I_{perp}:I_{para}, the ratio of the average intensity at a specific Q value in a 40° wide sector in the direction perpendicular to the magnetic field to that in the direction parallel to the field; Q, momentum transfer; R_c, radius of gyration of cross-section; R_g, radius of gyration; SDS, sodium dodecyl sulfate; TBE, Tris-Borate EDTA buffer; TMV, Tobacco Mosaic Virus; TRV, Tobacco Rattle Virus.

0006-3495/91/11/1178/12 $2.00

ferrimagnetic magnetite (Fe_3O_4) particles surrounded by a detergent bilayer suspended in an aqueous solvent whose pH and ionic conditions can be adjusted. The technique is well suited for neutron scattering studies where, unlike x-ray scattering studies, the signal from the ferrofluid particles can be greatly reduced by matching the neutron scattering length density of the ferrofluid particles to that of the solvent. The result is zero contrast between the ferrofluid particles and the solvent so that the neutron scattering is effectively from a uniform fluid. Contrast matching is accomplished through the use of deuterated ferrofluid components and a D_2O solvent.

This paper presents the results of studies done on three different systems. The first is TMV which is an ideal test system for the technique because it is a relatively rigid rodlike structure with an axial ratio greater than 10:1 and its structure is well known. The second is the less well characterized Tobacco Rattle Virus (TRV), which is morphologically similar to, but genetically distinct from TMV (7, 8). The third system we have studied is chromatin. Under physiological (150 mM) salt conditions, chromatin forms a filament known as the Higher Order Structure (HOS) which has a nominal diameter of 300 Å. At lower ionic strengths, the filament becomes more extended and disordered. How these different chromatin states relate to DNA replication, transcription, and storage is a topic of great interest. Many models for the HOS have been proposed including the cross-linker, solenoid, and superbead models (9–13). High quality neutron scattering on solutions of well-aligned chromatin filaments at various salt concentrations would help in evaluating these models. Additionally, they provide a test of whether the ferrofluid system is capable of aligning flexible structures. If so, the range of problems that can be addressed using the technique would be dramatically increased.

MATERIALS AND METHODS

Ferrofluid

The ferrofluid consists of particles with a magnetite (Fe_3O_4) core surrounded by a detergent bilayer suspended in D_2O or in H_2O. Two ferrofluids were prepared both using an ionic detergent, lauric acid (95% D, G & G Fine Chemicals, Reading, UK), for the inner detergent layer. The lauric acid head group binds to the magnetite core leaving the hydrocarbon portion on the exterior. To solubilize the aggregated hydrophobic particles a second detergent is added to form the outer layer of the bilayer. The two ferrofluids prepared used different deuterated detergents for the outer detergent layer: an ionic detergent, sodium dodecyl sulfate (SDS, 99% D, Flourochem LTD., Glossop Derbyshire, UK), and a nonionic detergent, LUBROL PX (99% D, MERCK, Sharp & Dohme Isotopes, Pointe Claire-Dorval, Canada).

The deuterated ferrofluids were prepared as follows. Approximately 90 ml of 10 M NaOD (99.9% D) was added slowly with stirring to a solution of 0.2 mol of hydrated ferric chloride and 0.1 mol of hydrated ferrous sulphate in D_2O. The mixture was heated to above 50°C before adding 8 g of perdeuterated lauric acid and left to stir for 1 h at room temperature, maintaining the pH between 9.5 and 10.0. The temperature of the mixture was raised to 95°C and allowed to cool. On acidification with DCl, the black suspension flocculated. The precipitate was washed with D_2O to remove residual salts followed by the addition of 2.5 g perdeuterated LUBROL PX or 2.5 g of perdeuterated SDS. The ferrofluid thus formed was centrifuged to remove large aggregates. The preparation of the nondeuterated ferrofluids was identical to the above preparation except the H replaced D throughout.

The saturation magnetization of the ferrofluid was measured using a vibrating sample magnetometer and the medium particle size was determined using electron microscopy.

Tobacco mosaic virus and tobacco rattle virus

The TMV and TRV (strain *campinas*) samples were prepared as described in references 14 and 15, respectively. Virus samples were initially in H_2O, and were exchanged into unbuffered 99.9% D_2O by repeated centrifugation (120 min at 163 kg) and resuspension. The neutron measurements were conducted on TMV (108 mg/ml) and TRV (112 mg/ml) diluted with an equal volume of deuterated ferrofluid made with LUBROL PX. All ferrofluid dilutions were done immediately before neutron measurements.

Chromatin

Concentrated (1–2 mg/ml) chicken erythrocyte chromatin samples were prepared in 80 mM NaCl, 10 mM Tris-HCl, pH 8.0, 1 mM Ethylenediaminetetraacetic acid (EDTA), and 0.2 mM phenylmethylsulfonyl fluoride (PMSF). Chromatin concentrations were determined by absorbance at 260 nm ($\epsilon_{260}^{1\%} = 20$). The DNA length had an average of 70,000 base pairs, determined by 1% agarose gel electrophoresis in 45 mM Tris-Borate, 1.25 mM EDTA Na_2 (TBE) buffer using a Bio-Rad CHEF gel apparatus. The sample was dialyzed four times against >99% D_2O. The samples used for neutron scattering measurements were prepared by mixing equal volumes of stock chromatin and deuterated LUBROL PX ferrofluid. The stability of nucleosomes was tested using a 5% polyacrylamide gel in 0.5 × TBE.

Electron microscopy

Measurements of the particle-size distributions of the ferrofluid were performed using an AEI Corinth 275 Electron Microscope. The electron micrographs produced (×3,000,000) were analyzed using a Zeiss Particle Size Analyzer (Jena, Germany). Virus samples were stained with 2% phosphotungstic acid at pH 7.0 and electron micrographs were recorded using a JEOL JEM-100s electron microscope (Tokyo).

Neutron scattering

Small-angle neutron scattering measurements on the ferrofluid and virus samples were conducted at the Institut Laue-Langevin (ILL) where the source of the neutrons is a nuclear reactor which continuously emits a spectrum of neutrons. At the D11 small-angle spectrometer (16), neutrons with a narrow range of incident wavelengths (typically $\Delta\lambda/\lambda = 8\%$) are selected using a helical slot monochromator. The monochromatic neutrons are scattered by the sample and are

recorded on a two-dimensional position-sensitive detector. The recorded position determines the scattering angle, 2θ, and the momentum transfer, Q, can be calculated using:

$$Q = \frac{4\pi \sin \theta}{\lambda}, \quad (1)$$

where λ is the neutron wavelength. Different angular, or Q, ranges can be measured by altering the distance, D, from the sample to the detector. Measurements were made with two different D and λ settings giving a low-Q range, 0.005–0.018 Å^{-1} (D = 10 m, λ = 10 Å), and a high-Q range, 0.10–0.34 Å^{-1} (D = 1.2 m, λ = 4.56 Å). The samples were measured in rectangular quartz cuvettes having a 1-mm path length. The beam size at the sample position was approximately 10 mm × 7 mm and the sample was large enough to completely fill this area.

The chromatin measurements used the Low-Q Diffractometer (LQD) at the Manuel Lujan Jr. Neutron Scattering Center (LANSCE) at Los Alamos National Laboratory which has a pulsed neutron source (17, 18). At a pulsed source, a very short burst of neutrons having a wide range of wavelengths is produced. LQD uses neutrons having wavelengths in the range 0.2–15 Å, and scattered neutrons are recorded on a two-dimensional position sensitive detector as a function of both time and scattering angle. Because all the neutrons are emitted at the same time, the wavelength of each can be determined from the time of its arrival at the two-dimensional detector. Using the measured wavelength and scattering angle, the momentum transfer can be calculated using Eq. 1 for each time slice and the resulting intensities summed. The wavelength distribution enables LQD to measure a wide range of Q values for a single detector position. The samples were measured in rectangular quartz cuvettes having a 1-mm path length. The beam size at the sample position was ~9 mm × 13 mm and the sample was large enough to completely fill this area.

Data analysis

The scattering data are presented as scattered neutron intensity per solid angle, $I(Q)$. The subtraction of the scattering from a ferrofluid background blank from that of the sample in ferrofluid removes, to first order, any contrast mismatch of the ferrofluid particles (6). The resulting difference profile is dominated by the biological particle of interest. Similarly, data for the ferrofluid particles with the appropriate H_2O or D_2O blank subtracted show scattering that is principally from the ferrofluid particles. The data shown here have the appropriate ferrofluid or buffer blank subtracted so that the scattering is primarily from the particle of interest, with the exception of the high-Q (1.2 m detector position) data from the ILL. For these data, a background is needed only to obtain the absolute height of a diffraction peak and this background level can be estimated from the data on either side of the peak.

In the small-angle region, the scattering profile can yield information about the size of the particle. At very low-Q, the scattered intensity profile can be approximated according to Guinier (19):

$$I(Q) = I(0)e^{-Q^2Rg^2/3}. \quad (2)$$

R_g is the radius of gyration of the particle and is defined as:

$$R_g^2 = \int_V [\rho_p(r) - \rho_s]r^2 dV \Big/ \int_V [\rho_p(r) - \rho_s]dV, \quad (3)$$

where $\rho_p(r)$ is the neutron scattering length density of the particle, ρ_s is the mean neutron scattering length density of the solvent, and V is the particle volume. The region of data where the Guinier approximation is valid varies according to the shape of the particle (20). For a spherical particle, it is valid over the Q-range for which $R_g \cdot Q \leq 1.3$. The R_g of a sphere of radius R is $\sqrt{0.6} \cdot R$ while the R_g for a thin rod of length L is $L/\sqrt{12}$.

When one dimension of the particle is much greater than the other two (e.g., a long rod), the scattering data can be scaled by Q to remove the longer distance from the data. This scaling yields a corresponding Guinier approximation for unoriented rodlike forms (19):

$$Q \cdot I(Q) = I_c(0)e^{-Q^2Rc^2/2}, \quad (4)$$

where R_c is the radius of gyration of cross-section of the particle and is defined as:

$$R_c^2 = \int_{Ac} [\rho_p(r) - \rho_s]r^2 dA_c \Big/ \int_{Ac} [\rho_p(r) - \rho_s]dA_c \quad (5)$$

and A_c is the cross-sectional area of the rod-shaped particle. A rod of radius R will have an R_c of $R/\sqrt{2}$. For oriented rods the scattering in the direction of the long axes of the rods will be at extremely low Q values and will therefore not be observable because of the very large length dimensions in that direction. The scattering perpendicular to the long axes of the rods will obey Eq. 4 (21). The range of Q for which Eq. 4 is valid depends not only on the shape of the cross-section but also on the aspect ratio of the rod (22). For infinite cylindrical rods, Eq. 4 is valid for $Q \leq 0.8/R_c$, but is often applicable up to $Q \leq 1.3/R_c$ with reasonable accuracy for elongated structures (20). However, the scattering from finite length rods will exhibit a decrease in intensity ("roll over") near the origin with decreasing Q. Explicitly, for rods of radius R with an aspect ratio, $A = L/(2 \cdot R)$, the scattering intensity will decrease for values of $Q < 5/(2 \cdot A \cdot R)$ (20). The higher the aspect ratio, the lower the value of Q where the roll over begins.

The degree of anisotropy in the two dimensional scattering data was evaluated using the ratio of the average intensity at a specific Q value in a 40° wide sector in the direction perpendicular to the magnetic field, $I_{perp}(Q)$, to that in the direction parallel to the magnetic field, $I_{para}(Q)$. In the absence of diffraction peaks, I_{perp}:I_{para} was calculated for Q = 0.01 Å^{-1}. For diffraction rings in the two-dimensional data I_{perp}:I_{para} was calculated for the Q value corresponding to the maximum intensity in the diffraction peak.

RESULTS

Ferrofluid

The distribution of values for the magnetite core diameter measured from electron micrographs was fitted to a normal distribution with a median of 83 Å and a standard deviation σ = 5 Å. The measured saturation magnetizations for the ferrofluids were typically 150 gauss.

Neutron scattering from dilute deuterated LUBROL PX ferrofluid (1:20 stock ferrofluid/water) was measured in both H_2O and D_2O (Fig. 1). The mean neutron scattering length densities for each molecular component of the ferrofluid are given in Table 1 (along with typical values for a protein and polynucleotide). The neutron scattering intensity for a particle in a homogeneous solvent is proportional to the contrast factor $\rho_p(r) - \rho_s$ (see Data Analysis). From the values given in Table 1, one expects both the LUBROL PX and the

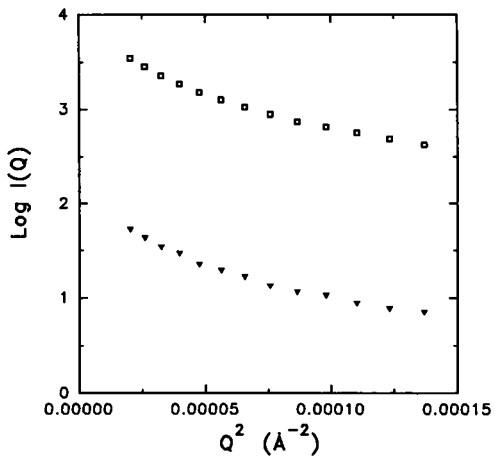

FIGURE 1 Guinier plot for blank subtracted scattering from dilute (5–6% by volume) deuterated Lubrol PX ferrofluid particles in H_2O (*squares*) and in D_2O (*triangles*) carrier fluid both in 0 magnetic field.

magnetite core to contribute significantly to the scattering from the deuterated ferrofluid in H_2O. In D_2O, the contribution of the LUBROL PX to the scattering is expected to be negligible, while the magnetite will give rise to a small but measureable signal.

Table 2 summarizes the zero angle scatter, $I(0)$, and radius of gyration, R_g, values calculated from scattering data from ferrofluid particles in H_2O and in D_2O. As expected, the scattering from the ferrofluid particles in H_2O was significantly greater than that from the ferrofluid particles in D_2O. In either solvent, the R_g was greater than 250 Å and thus fits could only be performed for values of $R_g \cdot Q \geq 1.3$ which is beyond the region where the Guinier approximation is strictly valid. However, the scattering data do indicate that the ferrofluid particles have aggregated because an individual particle in D_2O is expected to have an $R_g = 32$ Å, based upon the magnetite core diameter of 83 ± 5 Å determined from the electron microscopy. Filaments of ferrofluid have been observed in the presence of a magnetic field using optical microscopy (Charles, S. W., unpublished results) and it is known that ferromagnetic particles can form elongated chains (23). Hence, the D_2O and H_2O ferrofluid scattering data were also analyzed appropriately for rodlike forms to determine if the particles formed elongated aggregates under the current experimental conditions. The Guinier plots for rodlike forms in Figs. 2 and 3 show linear regions at low Q indicative of elongated assemblies of ferrofluid particles being present. The resulting R_c values are also given in Table 2. The expected R_c for a perfectly linear chain of spherical ferrofluid particles in D_2O is 26 Å, assuming the structure can be reasonably approximated as a rod of diameter 83 Å (see Data Analysis in Materials and Methods). The R_c determined from the more dilute D_2O ferrofluid neutron scattering data, which are dominated by contributions from the magnetite, are much larger than this indicating that the ferrofluid particles form more complex aggregates than simple linear chains. The scattering data for the more concentrated D_2O ferrofluid sample gave values for the R_g and R_c that are smaller than those determined for the dilute ferrofluid samples (Table 2),

TABLE 1 Scattering length densities

Component	Scattering length density
	cm^{-2}
Deuterated LUBROL PX	6.50×10^{10}
Magnetite	7.24×10^{10}
D_2O	6.30×10^{10}
H_2O	-0.56×10^{10}
"Typical" protein	$\approx 2.0 \times 10^{10}$
"Typical" polynucleotide	$\approx 3.8 \times 10^{10}$

Scattering length densities were calculated as $\Sigma\, b_i/V$ where the b_i's are the neutron scattering lengths for each atom in the molecule and V is the molecular volume.

TABLE 2 Fitting parameters for deuterated LUBROL PX ferrofluid particles in zero field

Sample	R_g‡	$I(0)$	Reduced χ^2	*DoF**	Q range ($Å^{-1}$)	$Q_{max} \cdot R_g$
1:20 DFF/H_2O	303 ± 6 Å	6,227	2.6	1	0.005–0.007	2.1
1:20 DFF/D_2O	286 ± 16 Å	85	1.43	1	0.005–0.007	2.0
1:1 DFF/D_2O	245 ± 7 Å	924	0.34	1	0.005–0.007	1.7
Sample	R_c‡	$I_c(0)$	Reduced χ^2	DoF*	Q range ($Å^{-1}$)	$Q_{max} \cdot R_c$
1:20 DFF/H_2O	175 ± 7 Å	21.4	0.6	1	0.005–0.007	1.2
1:20 DFF/D_2O	154 ± 20 Å	0.3	0.8	1	0.005–0.007	1.1
1:1 DFF/D_2O	91 ± 2 Å	3.5	3.5	4	0.010–0.014	1.3

Note that although the Guinier fits were all done using only the lowest Q data, the values of $Q_{max} \cdot R_g$ and $Q_{max} \cdot R_c$ for some data sets are larger than is ideal. This may result in values slightly different to the true values.

*DoF = degrees of freedom.

‡R_g is radius of gyration, and R_c is radius of gyration of cross-section.

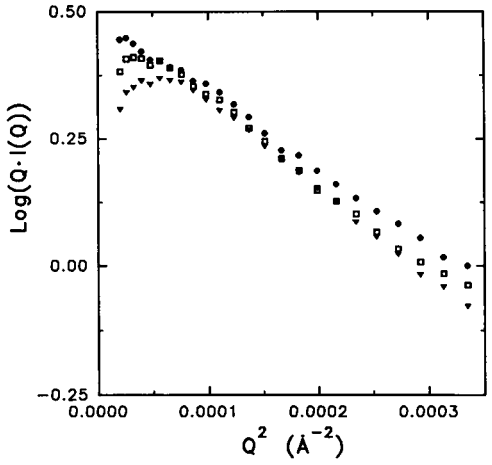

FIGURE 2 Guinier plot for rods on circularly averaged scattering of concentrated (50% by volume) deuterated Lubrol PX ferrofluid particles in D_2O in 0 kG (*circles*), 3 kG (*squares*), and 5 kG (*triangles*) fields.

though the R_c value is still much larger than the predicted value for a simple linear chain. In this more concentrated ferrofluid sample, the linear region of the Guinier plot extended to the lowest Q value measured indicating the aspect ratio of the aggregates was at least 5. In conclusion, the scattering data indicate that in both the dilute and concentrated ferrofluid samples elongated aggregates of magnetic particles having cross-sections greater than that of a single ferrofluid particle are present. However, such measurements do not preclude the presence of larger aggregates that would give rise to scattering at Q values below the measured range.

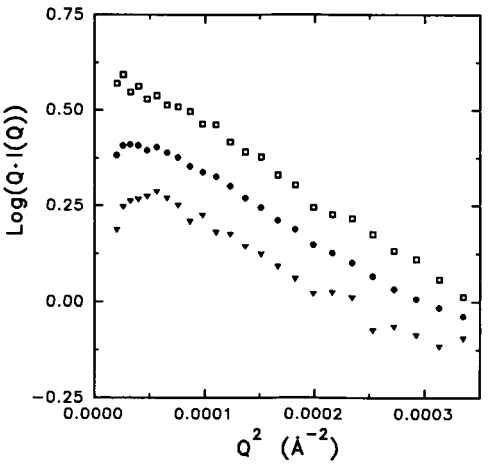

FIGURE 3 Guinier plot for concentrated (50% by ferrofluid volume) deuterated Lubrol PX ferrofluid particles in D_2O; circular average (*circles*), 40° wide sector perpendicular (*squares*), and parallel (*triangles*) to 3 kG field.

The application of a magnetic field to the more concentrated ferrofluid sample caused no significant change in the circularly averaged data (Table 3) except for a slight decrease in intensity for $Q < 0.01$ Å^{-1} (Fig. 2). The scattering from the ferrofluid exhibited anisotropy only when a magnetic field was applied (Fig. 3). The degree of anisotropy, I_{perp}:I_{para} at $Q = 0.01$ Å^{-1}, was 1.7:1 in the 3 kG field. The calculated R_c's for the parallel and perpendicular sectors were very similar but there was a slight increase in the degree of roll over below $Q = 0.01$ Å^{-1} in the direction parallel to the field, indicating (see Data Analysis) that the aspect ratio of the aggregates is the highest in the direction parallel and shortest in the direction perpendicular to the field. Otherwise, the scattering curve in any direction had nearly the same shape for $Q > 0.01$ Å^{-1} differing only by a scale factor from the scattering in any other direction; i.e., $I_{perp}(Q) \approx 1.7 \cdot I_{para}(Q)$. The degree of anisotropy increased slightly to 1.8:1 when the field was increased to 5 kG.

Tobacco mosaic virus

TMV is a rod-shaped virus, 3,000 Å long and 180 Å in diameter with a central hole of diameter 40 Å. Approximately 2,130 identical protein subunits of molecular weight 17,500 form a right-handed helix of pitch 23 Å, with 49 subunits in three turns. A single strand of RNA follows the basic helix between the protein subunits at a radius of 40 Å. A strong Bragg diffraction peak at $Q = 0.27$ Å^{-1} arising from the 23 Å pitch of the helix has been observed (2). Other peaks have been observed that correspond to the maxima of a first order Bessel function appropriate for the scattering from a hollow rod with a diameter of 180 Å.

To assess the structural integrity of the TMV in

TABLE 3 **Fitting parameters for deuterated LUBROL PX ferrofluid particles in D_2O (1:1)**

Magnetic field	Direction	R_c	$I_c(0)$	Reduced χ^2
kG				
0	Circ. aver.	91 ± 2 Å	3.5	3.5
3	Circ. aver.	95 ± 2 Å	3.5	0.6
3	Parallel	90 ± 4 Å	2.4	0.7
3	Perpendicular	98 ± 3 Å	4.8	1.5
5	Circ. aver.	90 ± 2 Å	3.2	0.9
5	Parallel	90 ± 4 Å	2.3	1.2
5	Perpendicular	98 ± 3 Å	4.9	0.6

The fits were performed over the Q range of 0.010–0.014 (Å^{-1}) with $DoF = 4$ and $Q_{max} \cdot R_c \approx 1.3$.

ferrofluid, electron micrographs were taken. Initial experiments used a ferrofluid which had an ionic detergent, SDS, as the outer detergent layer. Electron micrographs (data not shown) show the virus particles to have expanded in an irregular fashion indicating that the SDS ferrofluid severely perturbed the structure. A second ferrofluid which had the nonionic detergent LUBROL PX as the outer detergent layer did not cause any change in the morphology of the virus particles. Electron micrographs (data not shown) showed the virus to be a smooth and regular rod of the appropriate diameter and length for the normal structure. The LUBROL PX ferrofluid was used in all subsequent neutron experiments on the TMV and TRV samples.

Neutron scattering data were measured at two detector positions, 1.2 and 10 m, corresponding to Q ranges of 0.1–0.35 $Å^{-1}$ and 0.005–0.018 $Å^{-1}$. In the lower Q range, a single diffraction peak was observed at $Q = 0.017$ $Å^{-1}$ in zero field (Fig. 4 *a*). This corresponds to a Bragg distance of 360 Å and is consistent with a uniform interparticle distance associated with a nematic liquid crystal phase, which TMV is known to adopt in low ionic strength solutions (4). Liquid crystal domains form because the negatively charged TMV rods align parallel to each other at a uniform packing distance. This peak in the Guinier region precluded a Guinier analysis on these data. In zero magnetic field, the scattering from the diffraction peak was isotropic indicating no preferred orientation of the rods. Upon application of a 5-kG magnetic field, the peak associated with the interparticle distance aligned in the direction perpendicular to the applied field (Fig. 4 *b*), indicating the rods aligned with their long axes in the direction parallel to the field.

At the higher Q range in a 5-kG magnetic field, a strong diffraction peak was observed at $Q = 0.27$ $Å^{-1}$ on the meridian and a very weak peak at 0.14 $Å^{-1}$ on the equator (Fig. 4 *c*). The first peak arises from the 23 Å helical pitch of TMV and the weak peak is assignable to the third Bessel function maximum of the 180 Å diameter hollow structure. These data are consistent with the conclusion that the ferrofluid did not alter the structure of the virus. Again, in the presence of a magnetic field, the scattering was anisotropic (Fig. 4 *c*). The peak arising from the helical pitch oriented in the direction parallel to the applied field while the peak from the diameter oriented perpendicular to the field. This is expected for TMV particles aligned with the long axis of the virus parallel to the field and is consistent with the orientation of liquid crystal peak. The degree of anisotropy, I_{perp}:I_{para}, was ~10:1 for the peak from the helical pitch but was ~35:1 for the peak arising from the liquid crystal packing of TMV. Decreasing the applied field to 3 kG decreased the anisotropy of the liquid crystal peak to 33:1.

TMV has a large diamagnetic moment and is known to align in strong magnetic fields, typically greater than 20 kG (3, 4). The alignment is facilitated by the fact that TMV forms liquid crystal domains. To confirm that the alignment observed here was not due to the interaction between the modest fields used in the experiments and the intrinsic diamagnetic moment of TMV, scattering from TMV in D_2O alone at the same concentration, in and out of field, was measured at small momentum transfers. Two diffraction peaks were observed at Q = 0.009 and 0.016 $Å^{-1}$ corresponding to a distances of 710 and 390 Å indicating a different packing arrangement of the TMV rods in D_2O than in ferrofluid. The distances are consistent with nearest and next-nearest neighbor distances of the hexagonal nematic liquid crystal phase. A small degree of anisotropy, I_{perp}:I_{para} < 1.6:1 was observed before the field was applied and is believed to be caused by shear forces induced when the sample was pipetted into the cuvet. Importantly, the degree of anisotropy did not change upon application of the magnetic field indicating that the applied field was insufficient for the alignment observed in the presence of the ferrofluid.

Because counter-ions are known to disrupt the liquid crystal phase of TMV, a concentrated sodium phosphate buffer was added (final concentration, 10 mM $NaPO_4$) to the sample of TMV in the absence of ferrofluid. The low-Q range was measured and the diffraction peaks associated with liquid crystal packing disappeared. When a similar amount of the buffer was added to TMV plus ferrofluid sample, the scattering data, measured only at the high-Q range, still showed anisotropy consistent with alignment of the rods in the direction of the applied field. However, there was a factor of two decrease in the anisotropy of the diffraction peaks arising from the helical pitch.

Because there were no diffraction peaks from liquid crystal packing in the data from TMV with sodium phosphate in the absence of ferrofluid, a Guinier analysis could be performed (Table 4). The value of 61 ± 1 Å for R_c is very close to the value of 65 Å calculated for a uniform 180 Å diameter hollow rod having with inner diameter of 40 Å.

Tobacco rattle virus

Neutron scattering data from TRV in D_2O and in deuterated LUBROL PX ferrofluid showed no evidence for any liquid crystal domains, i.e., there were no diffraction peaks below $Q = 0.02$ $Å^{-1}$. Measurements of the TRV sample in ferrofluid using the high-Q (1.2 m) detector position showed a diffraction peak at 0.24 $Å^{-1}$,

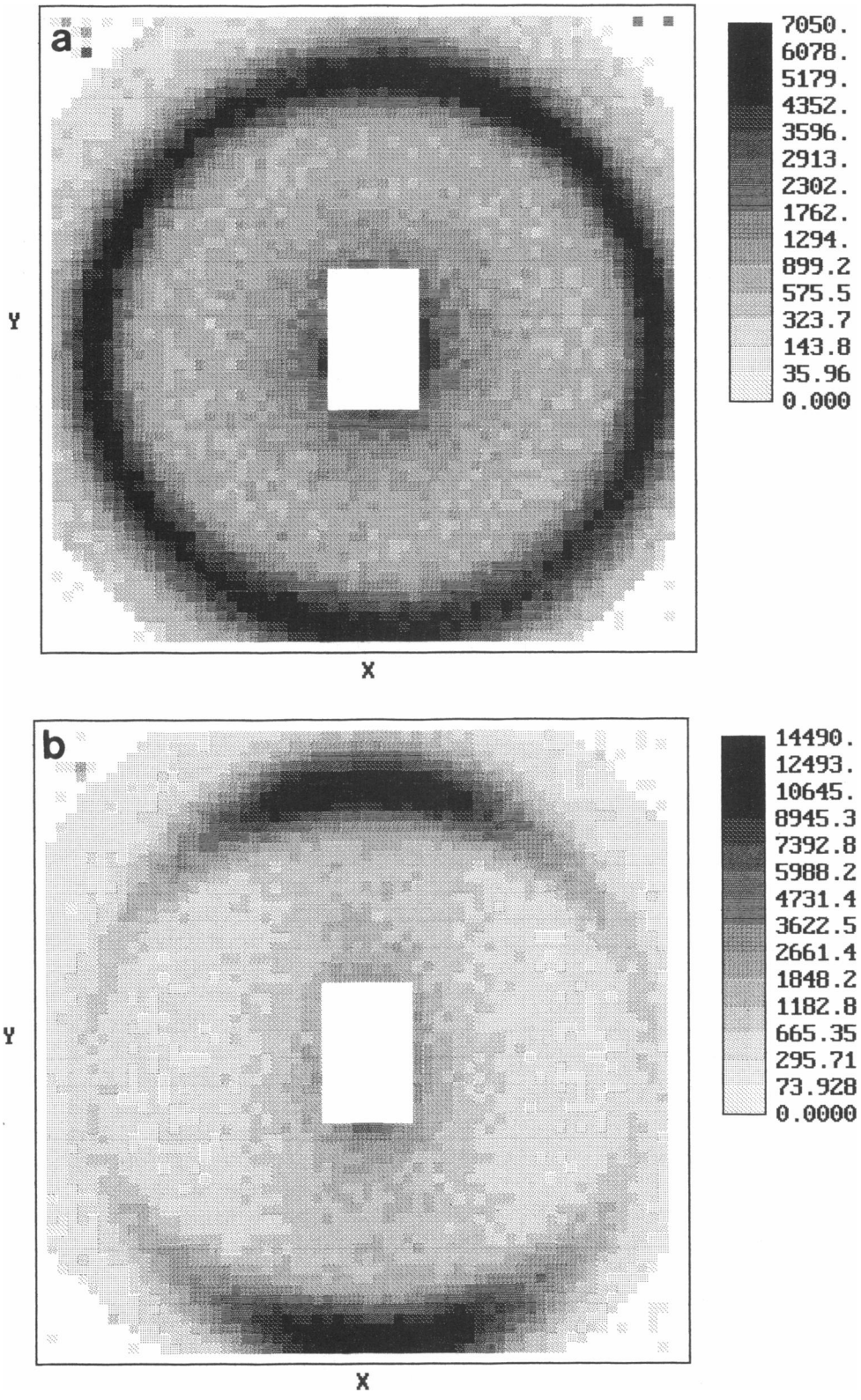

FIGURE 4 Two-dimensional plot of neutron scattering data for TMV in deuterated Lubrol PX ferrofluid (1:1) in D_2O with: (*a*) zero magnetic field, Q range 0.005–0.018 $Å^{-1}$; (*b*) for the same sample with a horizontal 3 kG magnetic field, Q range 0.005–0.018 $Å^{-1}$, and (*c*) the same sample in a 5 kG field, Q range 0.10–0.34 $Å^{-1}$; and (*d*) TRV in deuterated Lubrol PX ferrofluid (1:1) in D_2O with horizontal 5 kG magnetic field, Q range 0.10–0.34 $Å^{-1}$.

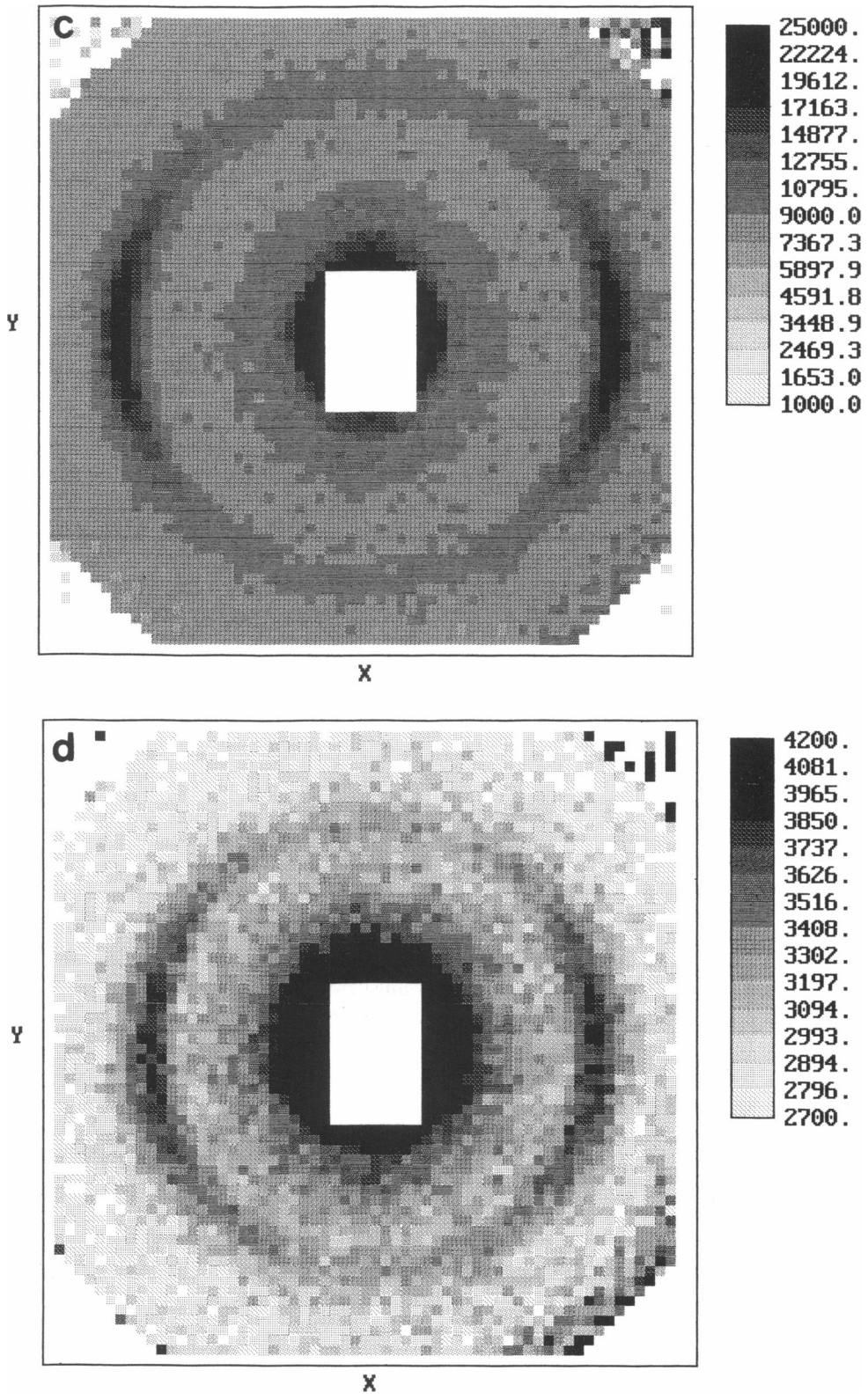

FIGURE 4 (continued)

TABLE 4 **Fitting parameters for TMV and TRV**

Sample	R_c	Reduced χ^2	*DoF*	Q range ($Å^{-1}$)	$Q_{max} \cdot R_c$
	Å				
1:1 TMV/D_2O with $NaPO_4$	61 ± 1	0.6	6	0.014–0.020	1.2
1:1 TRV/DFF in D_2O	91 ± 2	1.7	3	0.012–0.015	1.4
1:1 TRV/D_2O	91 ± 2	3.8	3	0.012–0.015	1.4

corresponding to a repeat distance of 26 Å (Fig. 4 *d*). This agrees with previous measurements of the helical pitch of TRV (25 Å according to data from Finch [7]). Because no diffraction peaks at very low Q were observed from the TRV samples in D_2O and in ferrofluid, a Guinier analysis for rodlike forms could be performed for both (Table 4). The calculated R_c was 91 ± 2 Å in D_2O and was 91 ± 2 Å in ferrofluid. These values agree well with expected R_c for TRV based on x-ray scattering data (7).

The scattering from TRV in ferrofluid was anisotropic only upon application of the magnetic field (Fig. 4 *d*). The diffraction peak assigned to the helical pitch aligned parallel to the applied field, similar to what was observed for TMV. The degree of ordering for the TRV rods was also similar to that observed in TMV after the addition of phosphate to that sample. The ratio I_{perp}:I_{para} for the diffraction peak was 5:1.

Chromatin

The stability of individual nucleosomes in ferrofluid was tested using a 5% polyacrylamide sizing gel. The addition of an equal volume of ferrofluid made with SDS or with LUBROL PX to a nucleosome sample (nominally 1 mg/ml) generated a distinct band containing only free DNA indicating that the ferrofluid caused some of the DNA to dissociate from the histones. When the experiment was repeated using chromatin fibers and the ferrofluid made with LUBROL PX, the chromatin remained intact. The LUBROL PX ferrofluid was used in the neutron scattering measurements.

The scattering from chromatin filaments in ferrofluid was measured in 40 mM NaCl, where it is believed to have a structure intermediate between the extended 100 Å filament and 300 Å fiber. I_{perp}:I_{para}, was <2 measured at $Q = 0.01$ $Å^{-1}$ indicating that the chromatin strands were aligning weakly in the direction parallel to the magnetic field (Fig. 5). The chromatin scattering shows a peak at $\sim Q = 0.012$ $Å^{-1}$. The peak is more pronounced in the direction parallel to the field (Fig. 5). The exact location of this low-Q peak is hard to determine because the peak is in the Guinier region and therefore superimposed on

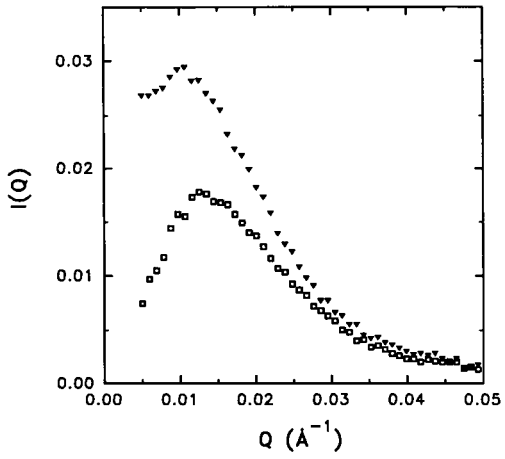

FIGURE 5 Neutron scattering data from chromatin in deuterated Lubrol PX ferrofluid (1:1) with the appropriate ferrofluid blank subtracted. The data were summed from 40° sectors parallel (*squares*) and perpendicular (*triangles*) to 2–3 kG field.

top of a steeply decreasing function. The presence of the diffraction peak in the Guinier region precludes a complete Guinier analysis. However, a value of R_c of 68.0 ± 0.8 Å was calculated using the negatively sloped data just to the right of the diffraction peak. These values and the general slope of the scattering curve are similar to x-ray scattering data of Bordas (12).

DISCUSSION

Anisotropic neutron scattering was observed for all three biological systems and for the ferrofluid itself. This anisotropy occurred only in the presence of both the ferrofluid and the magnetic field. The mechanism for ordering in ferrofluids is not clearly understood. Two possible mechanisms have been proposed (6). The first assumes that an asymmetric biological structure, by displacing ferrofluid particles, becomes a magnetic hole which reduces its magnetic energy by aligning parallel to the applied field (24, 25). This theory requires the structure be large enough to displace a sufficient number of ferrofluid particles that the ferrofluid can be considered to be a continuous ferromagnetic fluid. This is called the continuum limit. The second alignment theory argues that in magnetic fields, the ferrofluid particles form linear chains with their dipole moments parallel to the applied field (23, 26). To avoid the energetic costs of disrupting the chains, the biological structures align parallel to the chains and hence, are also aligned.

The linear chain argument is predicated on the ferrofluid particles forming linear chains in the direction

parallel to the applied field. In the Q range studied in the neutron scattering experiments, there is evidence for the existence of chain-like structures in the ferrofluid that scatter like filaments having an effective width greater than the diameter of a single ferrofluid particle in the absence and presence of a magnetic field. Also, the form of the anisotropy was such that the scattering in any direction had almost the same shape as the scattering in any other direction, differing only by an overall scale factor. One possible model that would explain both these features is that even without an applied field, ferrofluid particles form worm-like chains having an R_c greater than that from a simple chain. Upon application of a magnetic field, the chain-like structures tend to align parallel to the applied field. If this alignment were imperfect, i.e., part but not all of each filament aligned, the result would be rod-like scattering in both the parallel and perpendicular directions but with a different overall scale factor. This scale factor represents the ratio of the total length of the filaments that aligns parallel with the magnetic field to the total length that aligns perpendicular. One would expect that the length of the portions that remain perpendicular might become short enough that these segments are no longer in the infinite-rod limit, and the scattering would exhibit roll over (see Data Analysis) near the origin in the parallel direction. Roll over was observed only in the scattering in the parallel direction. The scattering data, however, do not preclude the presence of much larger aggregates, which have been observed by dynamic light scattering (Caroline, D., private communication), a.c. susceptibility measurements (27), optical microscopy, and sedimentation studies (Charles, S. W., unpublished results) all of which indicate that the ferrofluid contains aggregates with dimensions ≥ 500 Å.

It is not known definitively why the ferrofluid particles aggregate. Magnetic interactions appear to be insufficient because the ratio of the magnetic interaction energy between two ferrofluid particles to thermal energy is only 2:1 (given by $2\mu^2/R_{12}^3$: k_BT). This is supported by the observation that well dispersed magnetic particles of 85 Å diameter can be obtained in hydrocarbon carrier fluids. Aggregation could be attributed either to incomplete coverage of the particles by the secondary surfactant or to reduced effectiveness of the secondary surfactant as a disperant in aqueous media. Both possibilities can exist simultaneously. Nevertheless, the magnetic interactions are likely to be the cause of the chaining.

In considering the origin of the alignment of the biological assemblies, it should be noted that individual TRV particles or chromatin fibers are sufficiently small that they only displace on the order of one ferrofluid particle. Further, there is no evidence that the TRV or chromatin fibers form liquid crystal domains or any other type of aggregate. Hence for these systems the "continuum" model would not seem appropriate and another mechanism, possibly the "linear-chain" model, appears more likely. A definitive answer as to the alignment mechanism, however, will require further characterization of the structure of the ferrofluid.

The TMV data are more complex than the TRV and chromatin data because of the presence of liquid crystal domains of TMV particles in some samples. The liquid crystal phases were easily identified by the observation of diffraction peaks at very low Q corresponding to the interparticle spacings. The size of the liquid crystal domains is unknown, but they are likely to be large enough to exclude a sufficient number of ferrofluid particles to be considered in the continuum limit. Consequently, the premises of both the linear-chain and the continuum arguments are satisfied for the TMV liquid crystal domains and either or both theories might be valid. However, for the TMV data, the degree of anisotropy of the liquid crystal diffraction peaks was about three times greater than for the helical peaks. This implies that some of the virus rods were not in the liquid crystal phase; and, that the individual virus rods were not as well aligned as those rods in the liquid crystal domains. The increased alignment of the domains may be due to the domains entering the continuum limit where the alignment forces might be greater. Alternatively, the increased alignment may also be due to an increase in aspect ratio of the domains compared with that of individual rods.

An indication of the dependence of the degree of anisotropy on the dimensions of the aligned object can be inferred from the measurements taken of TMV in the presence of phosphate. The addition of phosphate to TMV in D_2O alone resulted in the loss of the low Q diffraction peaks associated with the liquid-crystal phase. A similar addition of phosphate to the TMV in ferrofluid reduced the anisotropy of the peaks associated with the helical pitch by a factor of two. Assuming that the addition of phosphate resulted in the disruption of the liquid-crystal domains in TMV in ferrofluid, the decreased alignment might be attributed to the alignment of single rods as opposed to liquid crystal domains. This view is supported by the fact that the degree of anisotropy was the same for TMV in phosphate plus ferrofluid as for the monodispersed TRV rods in ferrofluid.

The effects of the ferrofluid on the biological assemblies were minimal. The diffraction peaks from internal structures of both TMV and TRV in ferrofluid were identical to those observed by us and by others (2, 7) in the absence of ferrofluid. Also, the radius of gyration of cross-section for TRV did not change upon addition of ferrofluid. The ferrofluid did affect the liquid crystal

spacings in TMV. The spacings in D_2O alone were 390 and 710 Å which is consistent with nearest and next-nearest neighbor distances of a hexagonal nematic liquid crystal. The presence of the ferrofluid produced a single diffraction peak corresponding to a spacing 360 Å, which could also be attributed to hexagonal packing but with a smaller spacing.

The chromatin filaments aligned in the ferrofluid, but not as well as either of the two viruses, including TRV whose alignment may be attributed to the linear-chain mechanism. This is potentially the result of chromatin being a very loose and/or irregular flexible structure at 40 mM NaCl. This type of structure could, for example, bend around the chains of ferrofluid particles and not align as well as the more rigid virus rods. A diffraction peak was observed in the chromatin data at $Q < 0.015$ $Å^{-1}$ which is more pronounced in the direction of fiber axis (Fig. 5). This peak corresponds to a spacing greater than 400 Å, far larger than the linker length between nucleosomes. Similar peaks have been observed in x-ray data and used to support a loose three-dimensional model (12, 13) but the assignment of this peak is uncertain (28). Because the peak observed in this work was more pronounced along the fiber axis, it is unlikely that it is due to an interfiber distance. A possible explanation is the peak arises from a structural repeat along the fiber axis of a loosely wound helix.

In conclusion, we have demonstrated that biological structures that are difficult to align using conventional methods can be aligned using ferrofluids and modest magnetic fields. The ferrofluid technique is well suited to small-angle neutron scattering but not to x-ray scattering because the high iron content of the ferrofluid would produce a very strong signal in the x-ray beam. However, the technique might be extended to other biophysical methods which are not sensitive to iron, or which use very thin samples.

We wish to thank Philip Seeger for his assistance with the chromatin neutron scattering experiments using LQD. We also wish to thank Brian Imai for his assistance with the tests on the stability of the nucleosome core particles in ferrofluid. We wish to specially thank Roger Pynn and John Hayter for suggesting the ferrofluid technique might be useful for studying biological assemblies and for their encouragement and guidance in the initial investigations. Neutron scattering measurements were carried out at the Institut Laue-Langevin, Grenoble, France, and at the Manuel Lujan Jr. Neutron Scattering Center, a national user facility funded as such by the DOE/Office of Basic Energy Sciences.

This work was performed under the auspices of the DOE (contract W-7405-ENG-36) and was supported by DOE project KP-04-01-00-0 (Dr. Trewhella), National Science Foundation grant BBS8717949 (Dr. Stubbs), and DOE project DEFG03-88ER60673 (Dr. Bradbury).

REFERENCES

1. Namba, K., and G. Stubbs. 1985. Solving the phase problem in fiber diffraction. Applications to tobacco mosaic virus at 3.6 Å resolution. *Acta Cryst.* A41:252–262.
2. Namba, K., R. Pattanayck, and G. Stubbs. 1989. Visualization of protein-nucleic acid interactions in a virus. Refined structure of intact tobacco mosaic virus at 2.9 Å resolution by X-ray fiber diffraction. *J. Mol. Biol.* 208:307–325.
3. Cross, T. A., S. J. Opella, G. Stubbs, and D. I. D. Caspar. 1983. ^{31}P nuclear magnetic resonance of the RNA in tobacco mosaic virus. *J. Mol. Biol.* 170:1037–1043.
4. Oldenbourg, R., X. Wen, R. B. Meyer, and D. L. D. Casper. 1988. Orientational distribution function in nomatic tobacco-mosaic-virus liquid crystals measured by X-ray diffraction. *Phys. Rev. L.* 61:1851–1854.
5. Glucksman, M. J., R. D. Hay, and L. Makowski. 1986. X-ray Diffraction from magnetically oriented solutions of macromolecular assemblies. *Science (Lond.).* 231:1273–1276.
6. Hayter, J. B., R. Pynn, S. Charles, A. T. Skjeltorp, J. Trewhella, G. Stubbs, and P. Timmins. 1989. Ordered macromolecular structures in ferrofluid mixtures. *Phys. Rev. L.* 62:1667–1670.
7. Finch, J. T. 1965. Preliminary X-ray diffraction studies on tobacco rattle and barley stripe mosaic viruses. *J. Mol. Biol.* 12:612–619.
8. Harrison, B. D., and R. D. Woods. 1966. Serotypes and particle dimensions of tobacco rattle viruses from Europe and America. *Virology.* 28:610–620.
9. Williams, S. P., B. D. Athey, L. J. Muglia, R. S. Schappe, A. H. Glough, and J. P. Langmore. 1986. Chromatin fibers are left-handed double-helices with diameter and mass per unit length that depend on linker length. *Biophys. J.* 49:233–248.
10. Widom, J., and A. Klug. 1985. Structure of the 300 Å chromatin filament: x-ray diffraction from oriented samples. *Cell.* 43:207–213.
11. Bradbury, E. M., and J. P. Baldwin. 1986. Neutron scatter studies of chromatin structure. *In* Supramolecular Structure and Function. G. Pifat-Mrzljak, editor. Springer-Verlag, Berlin. 63–92.
12. Bordas, J., L. Perez-Grau, M. H. J. Koch, M. C. Vega, and C. Nave. 1986*a*. The superstructure of chromatin and its condensation mechanism. 1. Synchrotron radiation X-ray scattering results. *Eur. Biophys. J.* 13:157–173.
13. Bordas, J., L. Perez-Grau, M. H. J. Koch, M. C. Vega, and C. Nave. 1986*b*. The superstructure of chromatin and its condensation mechanism. II. Theoretical analysis of the X-ray scattering patterns and model calculations. *Eur. Biophys. J.* 13:175–185.
14. Noordan, D. 1973. Identification of Plant Viruses. Centre for Agricultural Publishing and Documentation, Wageningen, The Netherlands. 81 pp.
15. Huttinga, H. 1973. Separation of long and short particles of tobacco rattle virus with polyethylene glycol. *Neth. J. Plant Pathol.* 79:9–12.
16. Ibel, K. 1976. The neutron small-angle camera D11 at the high-flux reactor, Grenoble. *J. Appl. Cryst.* 9:296–309.
17. Seeger, P. A., R. P. Hjelm, and M. J. Nutter. 1990. The low Q diffractometer at the Los Alamos Neutron Scattering Center. *Mol. Cryst. Liq. Cryst.* 180A:101–117.
18. Seeger, P. A., A. Williams, and J. Trewhella. 1987. The low Q diffractometer at the Los Alamos Neutron Scattering Center. *In*

Proceedings of the International Collaboration on Advanced Neutron Sources IX SIN Report ISB 3-907990-01-4. F. Atchison, and W. Fischer, editors. Swiss Institute for Nuclear Research, Villigen. 437–447.

19. Guinier, A. 1939. La diffraction des rayons X aux très petits angles; application à létude de phénomènes ultramicroscopiques. *Ann. Phys. (Paris)*. 12:161–237.
20. Guinier, A., and G. Fournet. 1955. Small Angle Scattering of X-rays. John Wiley and Sons, New York. 128–129.
21. Glatter, O., and O. Kratky. 1982. Small Angle X-ray Scattering. Academic Press, London. 32–34.
22. Hjelm, R. P. 1985. The small-angle approximation of X-ray and neutron scatter from rigid rods of non-uniform cross section and finite length. *J. Appl. Cryst.* 18:452–460.
23. De Gennes, P. G., and P. A. Pincus. 1970. Pair correlations in a ferromagnetic colloid. *Phys. kondens. Materie.* 11:189–198.
24. Skjeltorp, A. T. 1983. One- and two-dimensional crystallization of magnetic holes. *Phys. Rev. L.* 51:2306–2309.
25. Skjeltorp, A. T. 1985. Ordering phenomena of particles dispersed in magnetic fluids (invited). *J. Appl. Phys.* 57:3285–3290.
26. Hayter, J. B., and R. Pynn. 1982. Structure factor of a magnetically saturated ferrofluid. *Phys. Rev. L.* 49:1103–1106.
27. Fannin, P. C., B. K. P. Scaife, and S. W. Charles. 1988. On the analysis of complex susceptibility data of ferrofluids. *J. Phys. D.* 21:1035–1036.
28. Greulich, K. O., E. Wachtel, J. Ausio, D. Seger, and H. Eisenberg. 1987. Transition of chromatin from the "10 nm" lower order structure, to the "30 nm" higher order structure as followed by low angle X-ray scattering. *J. Mol. Biol.* 193:709–721.